European Journal of Medicinal Chemistry 208 (2020) 112782

Contents lists available at ScienceDirect

European Journal of Medicinal Chemistry

journal homepage: http://www.elsevier.com/locate/ejmech

# Discovery of 5-bromo-4-phenoxy-*N*-phenylpyrimidin-2-amine derivatives as novel ULK1 inhibitors that block autophagy and induce apoptosis in non-small cell lung cancer

Dejuan Sun [a], Zijian Yang [a], Yongqi Zhen [b], Yushang Yang [c], Yanmei Chen [a], Yong Yuan [c], Lan Zhang [b, **], Xiaoxi Zeng [d, ***], Lixia Chen [a, *]

[a] Key Laboratory of Structure-Based Drug Design & Discovery of Ministry of Education, Wuya College of Innovation, Shenyang Pharmaceutical University, Shenyang, 110016, China
[b] School of Life Science and Engineering, Southwest Jiaotong University, Chengdu, 610031, China
[c] Department of Thoracic Surgery, West China Hospital, Sichuan University, Chengdu, 610041, China
[d] West China Biomedical Big Data Center, West China Hospital, Sichuan University, Chengdu, 610041, China

ARTICLE INFO

*Article history:*
Received 15 January 2020
Received in revised form
20 August 2020
Accepted 20 August 2020
Available online 29 August 2020

*Keywords:*
Non-small cell lung cancer
ULK1 inhibitors
A549 cells
Autophagy
Apoptosis

ABSTRACT

UNC51-like kinase1 (ULK1) recruits its binding partners and initiates the autophagy process in cancer. ULK1 is significantly overexpressed in Non-small cell lung cancer (NSCLC) and negatively correlated with clinical prognosis in NSCLC patients. Based upon the binding features of ULK1, we explored the pharmacophore modeling to discover the common anchoring features. It was verified by synthesizing 5-bromo-4-phenoxy-*N*-phenylpyrimidin-2-amine derivatives, as well as subsequently elucidating the structure-activity relationships (SAR). Among all the obtained ULK1 inhibitors, 5-bromo-4-(2-fluoro-4-nitrophenoxy)-*N*-(3,4,5-trimethoxyphenyl) pyrimidin-2-amine (**3s**), was the most active one. The docking analysis was conducted to compare **3s** and SBI-0206965, which further elucidated the roles of the H-bond donor. This compound inhibited the proliferation of A549 cells and showed strong inhibitory activity against ULK1 kinase. Moreover, we found that compound **3s** could induce apoptosis while simultaneously blocking autophagy. Collectively, these findings shed new light on compound **3s** that would be utilized as a promising candidate drug for the future NSCLC therapy.



## 1. Introduction

Lung cancer is the low 5-year overall survival and most frequently diagnosed cancer. Almost 2.3 million new cases of lung cancer have been diagnosed in 2019 [1,2]. It is estimated that NSCLC accounts for 83% of lung cancer cases. Despite significant progress in cancer research and treatment, the 5-year survival rate of NSCLC patients is only 15% [3]. The high incidence and morbidity rate of lung cancer has continued to increase in the developed countries. Consequently, it is highly efficacious to explore more efficacious therapeutic agents to benefit patient survival and quality of life [4,5].

Autophagy, a conserved biological process of phagocytosis, can remove damaging organelles, and maintain stable and normal physiological activities [6,7]. The autophagic process is regulated by autophagy-related genes. Among them, autophagy-related gene 1 (Atg1), a serine/threonine protein kinase, acts as a promoter of autophagy and regulates autophagy-initiating function [8,9]. Autophagy participates in diverse diseases, including cancer. However, autophagy plays a dichotomous role in cancer. There is mounting evidence that inducing autophagy could be an effective approach to inhibit other important process in cells, such as mTOR signaling or other stress responses [10]. The fusion peptide, Tat-Beclin1 is reported as a specific autophagy inducer [11]. Most researches reported that autophagy inhibition could suppress the growth of advanced cancers. Hydroxychloroquine, the autophagy inhibitor is the clinically available drug [12]. Combined hydroxychloroquine with temsirolimus, doxorubicin or bortezomib in patients with refractory solid tumors, including melanoma and glioblastoma multiforme [13,14].

* Corresponding author.
** Corresponding author.
*** Corresponding author.
*E-mail addresses:* zhanglanx_9@126.com (L. Zhang), zengxiaoxi@wchscu.cn (X. Zeng), syzyclx@163.com (L. Chen).

https://doi.org/10.1016/j.ejmech.2020.112782
0223-5234/

UNC-51 like kinase 1 (ULK1), Atg1 homologue, localizes to the autophagosomal membrane in mammalian cells and is diffusely reported as the autophagic initiator [15,16]. ULK1 is component of ULK1 complex (ULK1-ATF13-FIP200-ATG101), which plays an important role in autophagy induction. Characterization of ULK1 expression has been identified that up-regulation of ULK1 is found in some cancer tissues [17]. Previous study has reported that ULK1 showed up-regulated in NSCLC and negatively correlated with prognosis in NSCLC patients. Otherwise, knockdown of ULK1 inhibited cell growth and enhanced the efficacy of cisplatin against NSCLC cells [18]. Knockdown of ULK1 or the inhibition of ULK1 by the selective inhibitor SBI0206965, inhibited cell proliferation, induced cell apoptosis and enhanced the sensitivity of cisplatin against NSCLC cells [17]. In this case, inhibition of ULK1 to regulate autophagy process may be an efficacious therapeutic strategy.

Hitherto, multiple ULK1 inhibitors have been reported and researched for potential cancer treatment. As shown in Fig. 1, compound **6**, a high affinity inhibitor of ULK1 ($IC_{50}$ = 8 nM), was selected from a high throughput of 764 compounds with a standard $^{32}$P-ATP radioactive assay. However, compound **6** did not have specificity for ULK1 and the usage could not be determined in follow-up study [19]. In order to further improve the selectivity of ULK1, the inhibitor with novel scaffold was found. Compound **3** was less suitable as an inhibitor of ULK1, although it showed good selectivity [20]. A TBK1 inhibitor, MRT67307 could inhibit ULK1 ($IC_{50}$ = 45 nM) and ULK2 ($IC_{50}$ = 38 nM). Its homologue MRT68921 also had a good affinity. Unfortunately, neither MRT67307 nor MRT68921 had the specificity of ULK1. In addition, a high-throughput screening and structural modification revealed a ULK1 inhibitor having a skeleton of an anthracene derivative [21]. Compound **3g** had a potent affinity for ULK1 ($IC_{50}$ = 45 nM), which was consistent with MRT67307. WP1130 inhibited deubiquitinases, resulting in an increase in ULK1 ubiquitination, thereby inhibiting the activity of ULK1 and autophagy [22]. A FAK inhibitor, SBI-0206965, was also an inhibitor of high selectivity for ULK1 ($IC_{50}$ = 108 nM) and ULK2 ($IC_{50}$ = 711 nM). SBI-0206965 could inhibit ULK1 phosphorylation of VPS34 to regulate autophagy and cell survival [23].

Pharmacophore modeling was well applied in the field of medicinal chemistry [24,25]. Given several active molecules and favorable interactions with the active site, ligand-based pharmacophore elucidated comprehensive chemical features [26,27]. To introduce the method to understand development of ULK1-inhibitors and explore structure-activity relationship (SAR), we explored the pharmacophore modeling to discover the common anchoring features. In regrading to this, we further designed and synthesized a series of new ULK1 inhibitors according to the structure of ULK1 inhibitors in the literature, and finally 27 new small-molecule compounds were obtained. By studying the biological activity of these compounds, we found that **3s** not only had good inhibitory activity against tumor cells, but also showed strong inhibitory activity against ULK1 kinase. Subsequently, we carried out the SAR analysis and molecular docking. Further results revealed that **3s** blocked autophagy by ULK1 inhibition and induced apoptosis in human lung carcinoma A549 cells, which would shed new light on accelerating inhibitor discovery process of ULK1 and exploiting potential candidate drug for the future NSCLC therapy.

## 2. Results

### 2.1. Design and chemistry

ULK1 possesses the standard kinase fold, but still exists several unique features. The most notably feature is the large loop between the *N*- and C-terminal lobes, which has substrate recognition and kinase activity regulation. The positively charged loop extends out from the kinase domain, which is rare in the remainder of the kinome. Otherwise, ULK1 and ULK2 are the highly similar, while the loop is one of the most nonconserved features [28]. The skeleton of many inhibitors is similar to adenine, such as imatinib, infigratinib

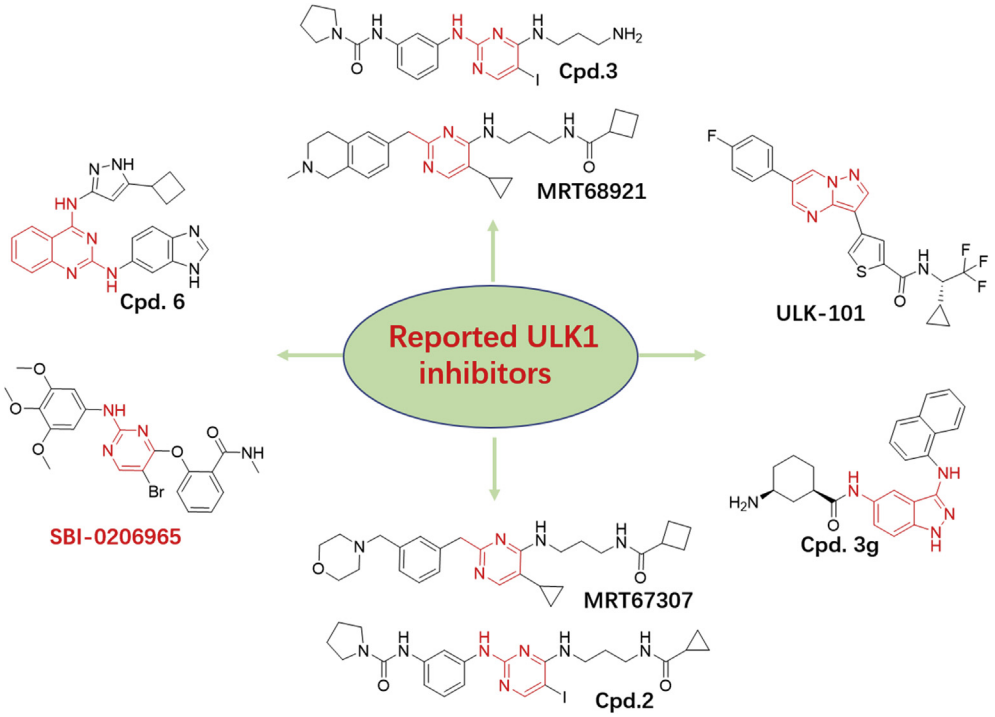


**Fig. 1.** The structures of reported ULK1 inhibitors.

and lapatinib. Here we constructed the pharmacophore modeling, which compared ligand-protein interactions and explored SAR (Fig. 2). In the first step, we read 3D coordinates of the ULK1 inhibitors-protein complex. ULK1 inhibitors were docked into the active site of ULK1 (PDB: 4WNO) (Fig. S1A). In order to nicely matching molecules, an overlap factor, hydrophobicity of protein cavities was introduced (Fig. S1B). The top1 pose was generated for each ligand. It was important to analyze the binding characteristics of reported ULK1 inhibitors. Firstly, based on the integrated structural features of ULK1 reported inhibitors, we found that the 2-aminopyrimidine scaffolds exhibited typical type I interactions with kinase hinge backbones as adenine did. Then, the flexibility of the methionine gatekeeper exerted control over ULK1 inhibitor binding by restricting access to the ATP-binding site deep. Additional, according to the rigidity of the chemical structure, existing inhibitors can be divided into two categories. An aliphatic chain or an aromatic ring occupied at the 4-position of pyrimidine. Finally, a substituted aromatic ring located in the allosteric pocket and occupied the hydrophobic binding site. Hydrophobic electron-withdrawing groups in the adenine core enhanced potency. In the second step, the pharmacophore model was wrapped into a normalized analysis that expresses the similarity between the ULK1 inhibitors (Fig. S1C). Smaller molecules inevitably got good matching with the pharmacophore model. The pharmacophore characteristics of ULK1 inhibitors were analyzed preliminarily, and we further analyzed the atomic characteristics of SBI0206965. The structure of SBI0206965 was most consistent with the pharmacophore based "fit value" (Table S1). Otherwise, as it is mentioned above, SBI0206965 was more selective for ULK1. Consequently, close protein atoms were identified by multiple types of ligand-protein interactions (e.g., H-bond donors, H-bond acceptors, hydrophobicity, stacking, CH-π). We expanded close ligand-protein atom to circular fragments and found ULK1 inhibitors-protein complex fragment. To further inhibit the ULK1 binding, H-bond donor and hydrophobic segments played an important role. Hydrogen bond formed by H-bond donor was towards the back pocket targeting the residues at the gatekeeper to gatekeeper +3 position. Otherwise, the contributions of hydrophobicity also were favorable interactions.

We examined the effect of various substituted groups and synthesized a series of derivatives according to the synthetic routes outlined in Scheme 1. The synthesis of compounds **3a-l** was introduced by using commercially available 2-hydroxybenzoic acid as the starting material. The reaction of 2-hydroxybenzoic acid with methylamine in ethyl acetate yielded intermediate **1**. Intermediate **1** reacted with 5-bromo-2,4-dichloropyrimidine to afford intermediate **2**. Then it reacted with *para*-bromoaniline and diverse aniline, which was prepared by refluxing reaction of THF in *p*-TsA, to obtain final compounds **3a-l** with 53–72% yields.

The synthetic routes of compounds **3m-u** were depicted in Scheme 2. The final compounds were yielded by two steps from commercially available 5-bromo-2,4-dichloropyrimidine. First, the

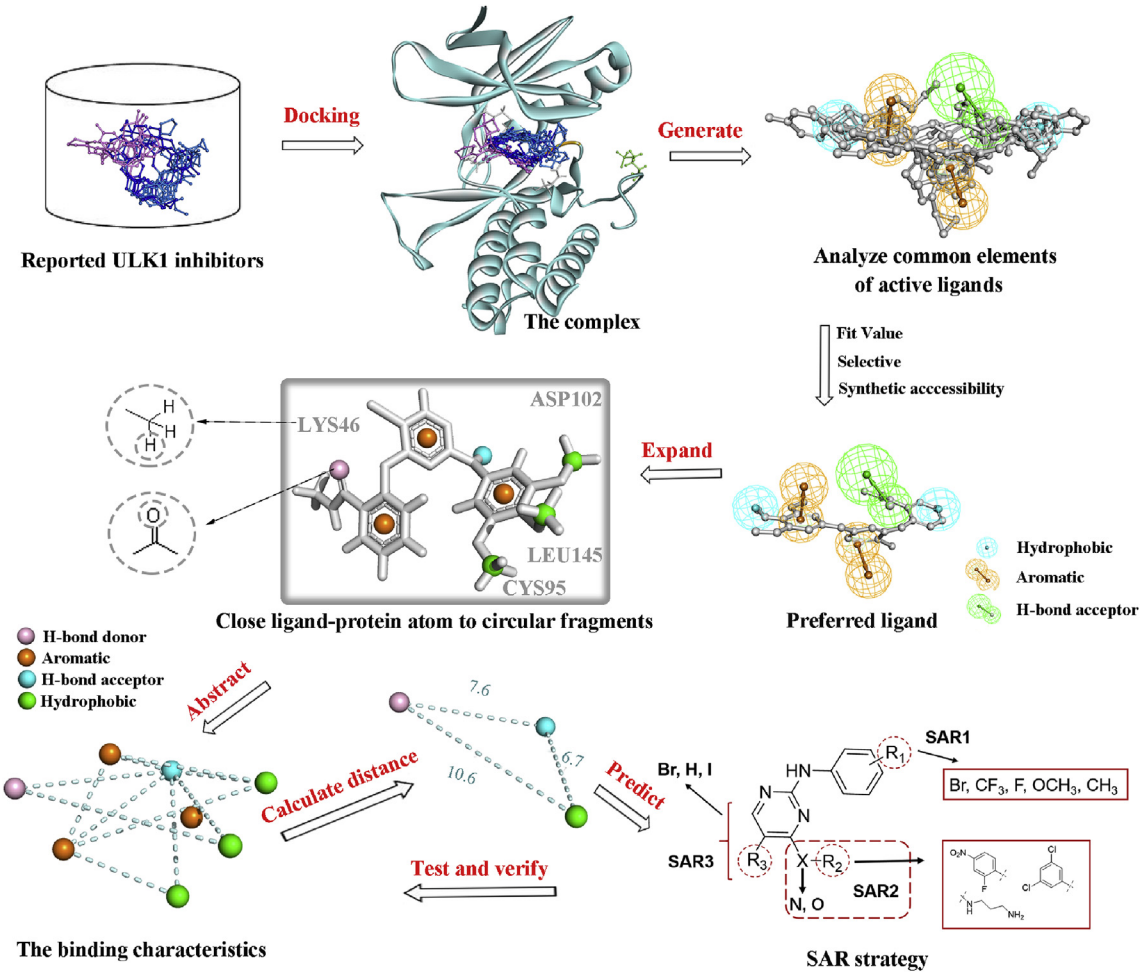


**Fig. 2.** The workflow of designing ULK1 inhibitors based on pharmacophore model.

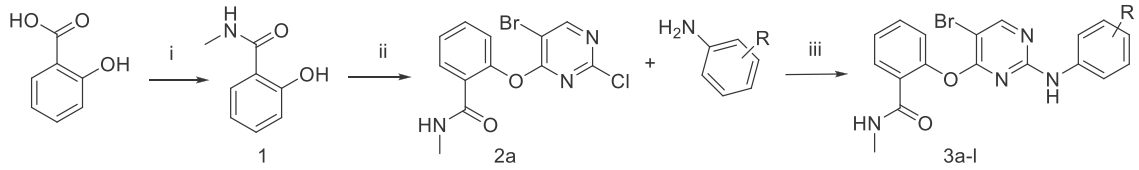

**Scheme 1.** Reagents and conditions: (i) Methanamine, 1-(3-Dimethylaminopropyl)-3-ethylcarbodiimide (EDCI), ethyl acetate (EA), r.t.; (ii) 5-bromo-2,4-dichloropyrimidine, *N*,*N*-Diisopropylethylamine (DIEA), Ethanol (EtOH), 0 °C to r.t.; (iii) *p*-Toluenesulfonic acid (*p*-TsA), Tetrahydrofuran (THF), reflux.

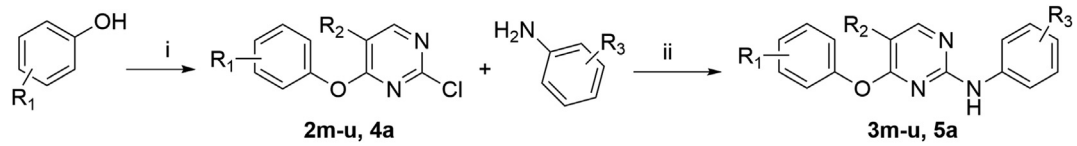

**Scheme 2.** Reagents and conditions: (i) 5-Bromo-2,4-dichloropyrimidine/Dichloropyrimidine, DIEA, EtOH, 0 °C to r.t.; (ii) *p*-TsA, $N_2$, THF, reflux.

preparation of compounds **2m-u** was employed by 5-bromo-2,4-dichloropyrimidine and diverse phenol in ethanol. Then, compounds **3m-u** were synthesized by the similar procedure as compounds **3a**. Compound **5a** was also synthesized by the similar method as **3a**.

In Scheme 3, **6a-c** was prepared via 2,4-dichloropyrimidine with *N*-Boc-1,3-propanediamine in isopropanol with $K_2CO_3$ at 80 °C. The desired compounds (**8a-c**) containing aliphatic chain were synthesized using **6a-c** with 3,4,5-trimethoxyaniline in the presence of THF and *p*-TsA. The *N*-Boc group was removed by Trifluoroacetic acid (TFA) in $CH_2Cl_2$ to provide the final compounds. Similarly, **10a-b** were carried out following reported procedures.

### 2.2. SAR analyses of the synthesized compounds

To examine SAR, kinase inhibition assay was utilized to assess the ability to inhibit ULK1. In the study, the following mainly three regions were focus on discussing the bioactivities effects (Fig. S2), including the skeleton structure, the head phenyl ether group (region I) and the terminal phenylamine group rings (region II). At first, anilines with different substituents were investigated (Table 1) on the bioactivity. For this purpose, we prepared a series of the aryl moieties introducing activity. All other parts of compounds were fixed as their original structures. A total of twelve compounds (**3a**-**l**) were synthesized.

Bioactivities of these compounds were listed in Table 1. Firstly, we introduced methoxy and fluorine substituents on ortho position. Unfortunately, the synthesized compounds showed no better activity than SBI0206965. For meta-position substituents, replacement of methyl (**3f**), methoxy (**3j**) and bromine (**3d**) exhibited a similar activity, whereas isopropyl substituent (**3k**) displayed higher affinity for ULK1. This suggested that electronegativity of substituents did not affect the potency for ULK1, which was depended on the chemical space. To further explore the space, we synthesized compound **3l**, which showed no activity. For para-position and di-substituents, these compounds displayed moderate activity with no significant improvement.

To further explore the potency for ULK1, we investigated the influence of the aryl moiety $R_1$ and $R_2$. Ten compounds (**3m**−**3u, 8a**) were synthesized, and structures and bioactivities of these compounds were shown in Table 2. According to the activity results of **3a-3l**, we chose 3-methylaniline/3,4,5-trimethoxyaniline fixed on region I. The possible influence of various substituted was surveyed in the subsequent structural modifications. We replaced *N*-methylaminocarbonyl with 2-ethoxyl substituent to assess the effect of a role of chemical space, which was weak activity towards ULK1. We investigated the effect of other electron-withdrawing substituents. The introduction of 3-fluoro, 3-nitro, 4-bromo and 2,4-dichloro substituents did not affect the potency for ULK1, which indicated that had no contribution to the achievement of activity.

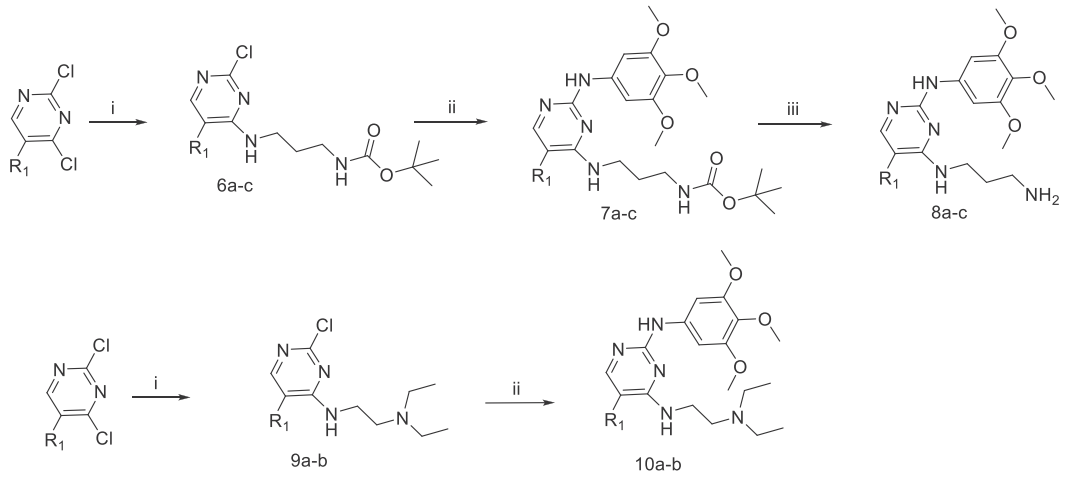

**Scheme 3.** Reagents and conditions: (i) Isopropanol, $K_2CO_3$.; reflux; (ii) 3,4,5-Trimethoxyaniline, THF, *p*-TsA, reflux; (iii) Trifluoroacetate, $CH_2Cl_2$, 0 °C to r.t.

**Table 1**
SAR study on the head phenyl ether group (region I).

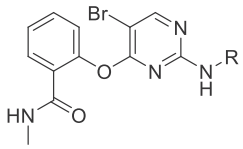


| NO. | R | Kinase inhibitory activity (10 μM, %)[a] | Anti-proliferative activity ($IC_{50}$, μM)[b] | | | | |
|---|---|---|---|---|---|---|---|
| | | | A549 | U937 | HL60 | MDA-MB-468 | MCF-7 |
| **3a** | 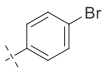 | 40.12 | 23.46 ± 1.75 | >50 | 39.69 ± 0.85 | 36.60 ± 1.75 | >50 |
| **3b** | 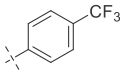 | 21.56 | >50 | >50 | >50 | >50 | >50 |
| **3c** |  | 27.42 | 35.46 ± 1.87 | >50 | >50 | >50 | >50 |
| **3d** | 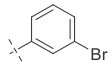 | 62.69 | 10.60 ± 1.20 | 49.00 ± 2.58 | 38.70 ± 1.66 | 31.90 ± 2.95 | 42.50 ± 2.53 |
| **3e** |  | 19.24 | 40.53 ± 1.38 | 52.13 ± 2.23 | >50 | >50 | >50 |
| **3f** |  | 73.68 | 6.10 ± 1.54 | 15.88 ± 3.06 | 16.21 ± 2.75 | 18.59 ± 1.96 | 16.55 ± 2.64 |
| **3g** | 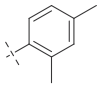 | 38.24 | 27.33 ± 3.12 | 49.6 ± 1.54 | 32.32 ± 1.88 | 40.7 ± 1.97 | 44.67 ± 2.24 |
| **3h** | 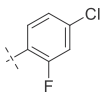 | 17.79 | 38.14 ± 0.95 | >50 | >50 | >50 | >50 |
| **3i** | 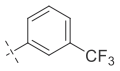 | 38.84 | 28.32 ± 2.64 | 45.53 ± 3.13 | 43.96 ± 1.45 | 32.82 ± 2.46 | 57.77 ± 1.95 |
| **3j** | 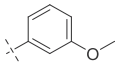 | 50.46 | 6.23 ± 2.31 | 24.33 ± 2.45 | 16.17 ± 2.89 | 17.76 ± 1.44 | 18.22 ± 2.56 |
| **3k** | 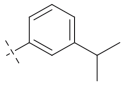 | 83.96 | 7.14 ± 1.58 | 14.05 ± 1.94 | 17.51 ± 1.48 | 19.45 ± 2.58 | 26.48 ± 1.84 |
| **3l** | 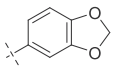 | 22.25 | >50 | >50 | >50 | >50 | >50 |
| **SBI-0206963** | 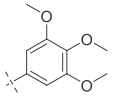 | 97.56 | 6.78 ± 1.58 | 25.12 ± 0.94 | 18.92 ± 1.7 | 18.38 ± 0.35 | 26.17 ± 0.35 |

[a] Each compound was tested in triplicate; the data are presented as the mean ± SEM (n = 3).
[b] $IC_{50}$ values obtained with cell viability assay for 24 h.

The results revealed that the electron-withdrawing group at 2, 3 or 4 position showed poor activity. However, **3s** presented a significant improvement of activity, owing to the 4-nitro substituent, which could interact with ULK1 closely. Otherwise, we designed to retain aliphatic amine to meet the flexible need.

To examine the possible influence of electronegativity of skeleton, different substituted pyrimidines were designed to explore the roles of 5-bromo. From Table 3, we found the electron-withdrawing substituent at 5 position showed the highest activity. In addition, considering the effect of alkylamines chains on the region II, we further designed compounds **8b-c**, **10a-b**. Among them, the best activity was **5a**, but obviously weaker than **3s**.

Based on the above data, we could conclude that hydrophobic interaction was more favorable on region I. Of special note was that

**Table 2**
SAR study on the terminal phenylamine group rings (region II).

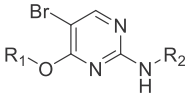

| NO. | $R_1$ | $R_2$ | Kinase inhibitory activity (10 μM, %) | Anti-proliferative activity ($IC_{50}$, μM) | | | | |
|---|---|---|---|---|---|---|---|---|
| | | | | A549 | U937 | HL60 | MDA-MB-468 | MCF-7 |
| **3m** | 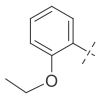 |  | 75.68 | 20.31 ± 1.06 | 38.64 ± 0.95 | 34.73 ± 0.73 | 31.40 ± 0.72 | 39.11 ± 1.32 |
| **3n** | 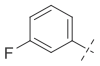 |  | 49.26 | 13.90 ± 2.49 | 19.36 ± 3.28 | 15.47 ± 2.59 | 29.21 ± 3.72 | 26.80 ± 2.49 |
| **3o** | 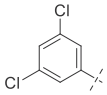 |  | 3.78 | 43.94 ± 1.49 | >50 | >50 | >50 | >50 |
| **3p** | 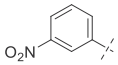 |  | 40.24 | 24.63 ± 2.47 | 51.23 ± 3.75 | 38.66 ± 1.48 | 36.68 ± 1.38 | >50 |
| **3q** | 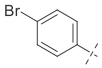 |  | 25.68 | 10.30 ± 0.34 | 18.64 ± 2.48 | 14.73 ± 1.58 | 31.32 ± 3.85 | 19.11 ± 2.5 |
| **3r** | 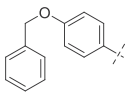 |  | 16.34 | 48.73 ± 0.34 | >50 | >50 | >50 | >50 |
| **3s** | 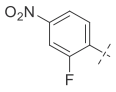 | 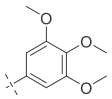 | 99.15 | 1.94 ± 2.35 | 12.92 ± 1.49 | 10.89 ± 0.98 | 16.83 ± 0.86 | 19.60 ± 2.38 |
| **3t** | 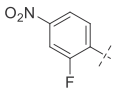 | 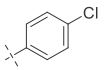 | 15.67 | 37.55 ± 1.44 | 43.09 ± 1.53 | >50 | >50 | >50 |
| **3u** | 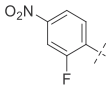 | 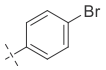 | 12.46 | 51.03 ± 1.64 | >50 | >50 | >50 | >50 |
| **8a** |  | 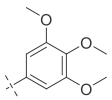 | 60.86 | 13.34 ± 1.44 | 20.65 ± 1.24 | 21.47 ± 2.15 | 33.12 ± 2.35 | 21.91 ± 2.15 |
| **SBI-0206963** | 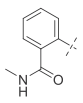 | 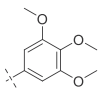 | 97.56 | 6.78 ± 1.58 | 25.12 ± 0.94 | 18.92 ± 1.7 | 18.38 ± 0.35 | 26.17 ± 0.35 |

**3s** showed the highest activity and had higher affinity for ULK1 than SBI0206965, also the cellular potency of **3s** was 3−4 higher. This compound contained a 2-fluoro-4-nitrophenyl ether group at the region II position and 3,4,5-trioxyl group at the region I position.

### 2.3. Identification of 3s as a new ULK1 inhibitor

The antiproliferative activity of synthesis compounds was presented in supporting Table 1. This study was performed on several human cancer cell lines A549, U937, HL60, MDA-MB-468 and MCF-7, which were derived from human lung, lymphoma, breast cancer and acute myeloid leukemia, respectively using MTT assay. The **3s** exhibited the highest cytotoxic effect against all the tested cell lines with $IC_{50}$ < 20 μM, while homologue **3t** was weaken anticancer activity with $IC_{50}$ ranged between 37.55 and 89.12 μM. Generally, compounds bearing ortho-substituents on region I **3c** and **3e** were devoid of anticancer activity. Meanwhile, the congeners having meta-substituents **3d** and **3f** exhibited good anticancer effects (Fig. 3A). The inhibitory activities of **3a-3u** against ULK1 were evaluated. For comparison, SBI0206965, the reported ULK1 inhibitor, was used as standard drug. The activity for the inhibition of ULK1 was summarized. The result showed that **3s** exhibited significant inhibitory activities on ULK1 (Fig. 3B). To further confirm the target selectivity of **3s**, a KINOME scan panel of 100 kinases binding assays was performed by Eurofins Pharma Discovery Services UK Limited. The results showed that **3s** prominently inhibited the kinase activity of ULK1, but still inhibited a number of kinases.

**Table 3**
SAR study on the skeleton and alkylamines chains.

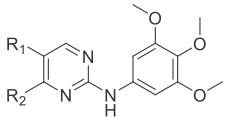

| NO. | $R_1$ | $R_2$ | Kinase inhibitory activity (10 μM, %) | Anti-proliferative activity ($IC_{50}$, μM) | | | | |
|---|---|---|---|---|---|---|---|---|
| | | | | A549 | U937 | HL60 | MDA-MB-468 | MCF-7 |
| **3s** | Br | 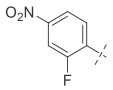 | 99.15 | 1.94 ± 2.35 | 12.92 ± 1.49 | 10.89 ± 0.98 | 16.83 ± 0.86 | 19.60 ± 2.38 |
| **5a** | H | 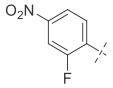 | 66.96 | 10.08 ± 2.54 | 23.12 ± 2.75 | 16.21 ± 2.67 | 20.37 ± 1.76 | 23.55 ± 2.24 |
| **8b** | H | 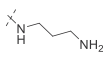 | 17.66 | 29.65 ± 1.71 | >50 | >50 | 45.78 ± 2.12 | >50 |
| **10a** | H |  | 13.41 | 46.39 ± 2.79 | >50 | >50 | >50 | >50 |
| **8c** | I | 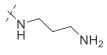 | 32.31 | 39.64 ± 2.45 | 39.93 ± 2.74 | 43.41 ± 3.63 | >50 | >50 |
| **10b** | I |  | 44.86 | 16.89 ± 1.29 | 21.96 ± 3.27 | 21.57 ± 3.34 | 32.27 ± 3.24 | 32.69 ± 1.29 |

Most notably, AMPKα1 and FAK were still targeted (Fig. 3C, Table S2). Furthermore, to confirm whether **3s** could inhibit the kinase activity of ULK1 in cells, we detect the cellular phosphorylated levels of ULK1 substrates such as Atg13 (Ser318) and Beclin1 (Ser15) under normal or nutrient starvation conditions. The results showed **3s** can inhibit ULK1 activity in A549 cells, as indicated by the decreased levels of *p*-Atg13$^{Ser318}$ and *p*-Beclin1$^{Ser15}$ (Fig. 3D).

### 2.4. Molecular docking

Molecular docking (MD) is a widely used approach to predict the predominant binding mode and screen potential active structures [29]. To explore structural information of ULK1 inhibitor binding modes, two kinase-inhibitor complexes were analyzed by MD. In the study, the crystal structure of ULK 1 kinase domain was obtained from the RCSB PDB database (http://www.rcsb.org, PDB entry: 4WNO, 1.56 Å resolution). Compound **3s** was selected as a potential ULK1 inhibitor, based upon the consideration of kinase inhibitory effect and anti-tumor activity. In order to investigate the interaction of **3s** with ULK1 and understand the conformation of **3s** in the active site, the analysis was conducted to compare **3s** and SBI-0206965. In this study, ligands with the most favorable binding free energies and reasonable orientations were chosen as the optimal docked conformation. We investigated that **3s** and SBI-0206965 could bind to ULK1 stably (Figs. S3A and B). Two inhibitors formed canonical hydrogen bonds with the hinge backbones. However, small differences were found in their binding positions. 2-Aminopyrimidine NHs of **3s** formed hydrogen bonds with backbone carbonyl (Cys95, the gatekeeper +3 position residue) of the ULK1 hinge region, while 2-aminopyrimidine moiety acted as an adenosine mimic, which was stronger interactions than SBI0206965. In addition, interactions between the nitro moiety on the region II and the backbone carbonyl of Gln142 also contributed to strong binding. Furthermore, the pocket formed by Ile22, Val30, Ala44 formed hydrophobic interactions with the region I group (Fig. 4). H-bond formed at gatekeeper +3 position restricted access to the ATP-binding site deep and was beneficial to improve the activity of ulk1 inhibitor. The results showed that H-bond donor and hydrophobic segments played an important role.

### 2.5. 3s blocks autophagy by ULK1 inhibition in A549 cells

ULK1 is closely related to early autophagosome formation, and phosphorylates beclin1 to trigger the autophagy cascade. So, inhibiting ULK1 possibly blocks autophagy. We detected the ability of **3s** to inhibit autophagy and cell survival in A549 lung cancer cells. The suppression of ULK1 expression was surveyed by immunoblotting. Firstly, we found that **3s** significantly downregulated the activity of ULK1 and induced downregulation of *p*-ULK1 (ser317) in a concentration-dependent manner (Fig. 5A). AMPK can directly activate ULK1 by phosphorylation at Ser317. So, the expression of ULK1 may be decreasing due to **3s** inhibition of AMPK. We also revealed that the LC3 conversion was significantly delayed in A549 cells. To confirm the result, autophagy flux was researched by p62 degradation assay. Treated with **3s**, p62 degradation was not observed in A549 cells, and the expression of beclin1 was decreased. As expected, treatment with **3s** resulted in a prominent inhibition of autophagy, as evidenced by an increase in the autophagy substrate p62, a reduction in LC3 I conversion to LC3 II, and a decrease in the levels of beclin1 (Fig. 5B). Taken together, the results suggested that inhibition of ULK1 kinase activity by **3s** blocked autophagy of A549 cells. To further assess autophagy, we looked at the autophagy flux by GFP-mRFP-LC3 (Fig. 5C). These results suggest that **3s** can block autophagy via inhibiting ULK.

### 2.6. 3s promotes apoptosis in A549 cells

ULK1 is closely to elucidate the mechanisms of **3s** -inhibited A549 cells growth, the morphologic changes were observed under inverted microscopy by Hoechst 33,258 staining. When cells were treated with **3s**, the apoptotic DNA fragments significantly increased in dose department manner (Fig. 6A). Subsequently,

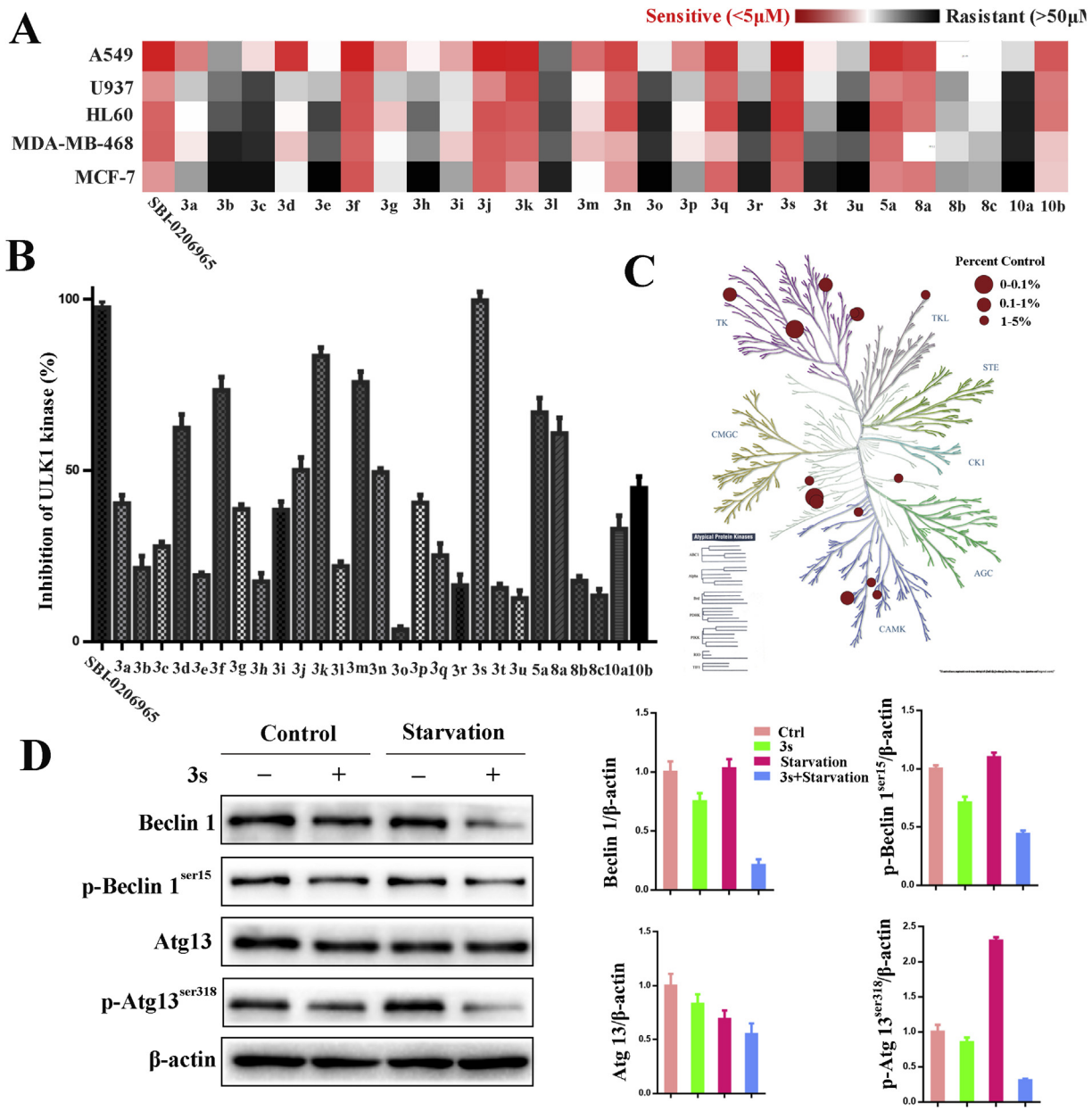


**Fig. 3. Identification of 3s as the ULK1 inhibitor.** (A) Treatment with a series of compounds after 24 h, anti-tumor viabilities were detected by MTT assay. (B) The kinase inhibitory activity of ULK1 for synthesized compounds and SBI020695 were detected by kinase assay at 10 μM. Kinases whose binding was inhibited by **3s** were marked with red circles, and the circle size indicates the degree of binding affinity. (C) Kinome tree represented the selectivity of **3s**. The activity of kinases was measured in the presence of 10 μM **3s**. (D) A549 cells were treated with **3s**, under normal or nutrient starvation conditions. After treatment, the expression levels of Beclin 1, *p*-Beclin1$^{Ser15}$, Atg13, *p*-Atg13$^{Ser318}$ were analyzed by immunoblotting, β-actin was used as a loading control. (For interpretation of the references to color in this figure legend, the reader is referred to the Web version of this article.)

Western blot analysis revealed that bcl-2 expression was remarkably down-regulated, bax and the active form of caspase-3 expression were increased after **3s** treatment (Fig. 6B). Taken together, these results indicated that **3s** could induce apoptosis via the mitochondrial pathways in A549 cells.

## 3. Conclusions

ULK1, a well-known autophagy initiator, has been reported to be significantly up-regulated in NSCLC and negatively correlated with clinical prognosis of patients. Consequently, discovery of new ULK1 inhibitors will be a promising strategy for the current NSCLC treatment. We explored the pharmacophore modeling to discover the common anchoring features, which derived the inhibitor discovery process of ULK1, including: (i) the identification of common anchoring features of the ULK1-inhibitors interactions; (ii) the analysis of the influence of chemical features and the interpretation of SAR by focusing on structural modifications; (iii) the favorable interactions of improving the true odds of high-throughput virtual screening. Subsequently, the experiments were performed on compound synthesis, screening, and mechanism of action. The results indicate that compound **3s** displays a remarkable inhibitory activity against ULK1, but still targeted other kinases, including FAK, Src, JAK3 and AMPKα1. Otherwise, compound **3s** inhibits the proliferation of A549 cells in a concentration-dependent manner, which is much stronger than a known ULK1 inhibitor SBI0206965.

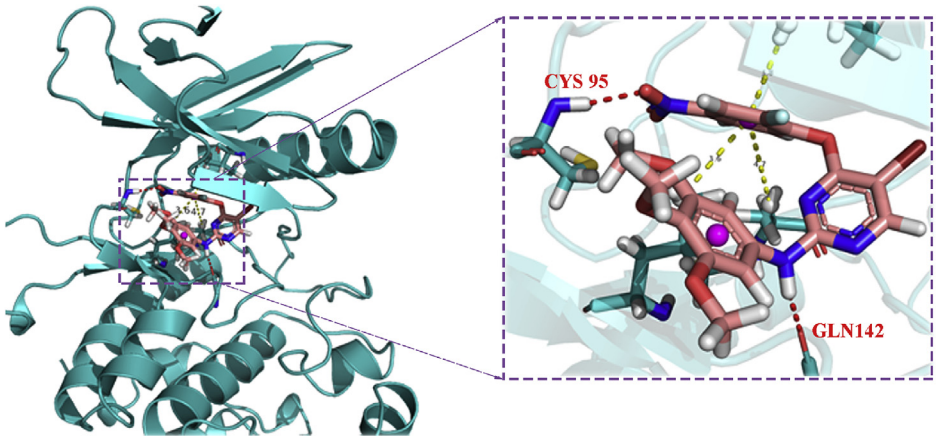


**Fig. 4.** Predicted binding mode of compound 3s in the active of ULK1 (PDB: 4WNO2).

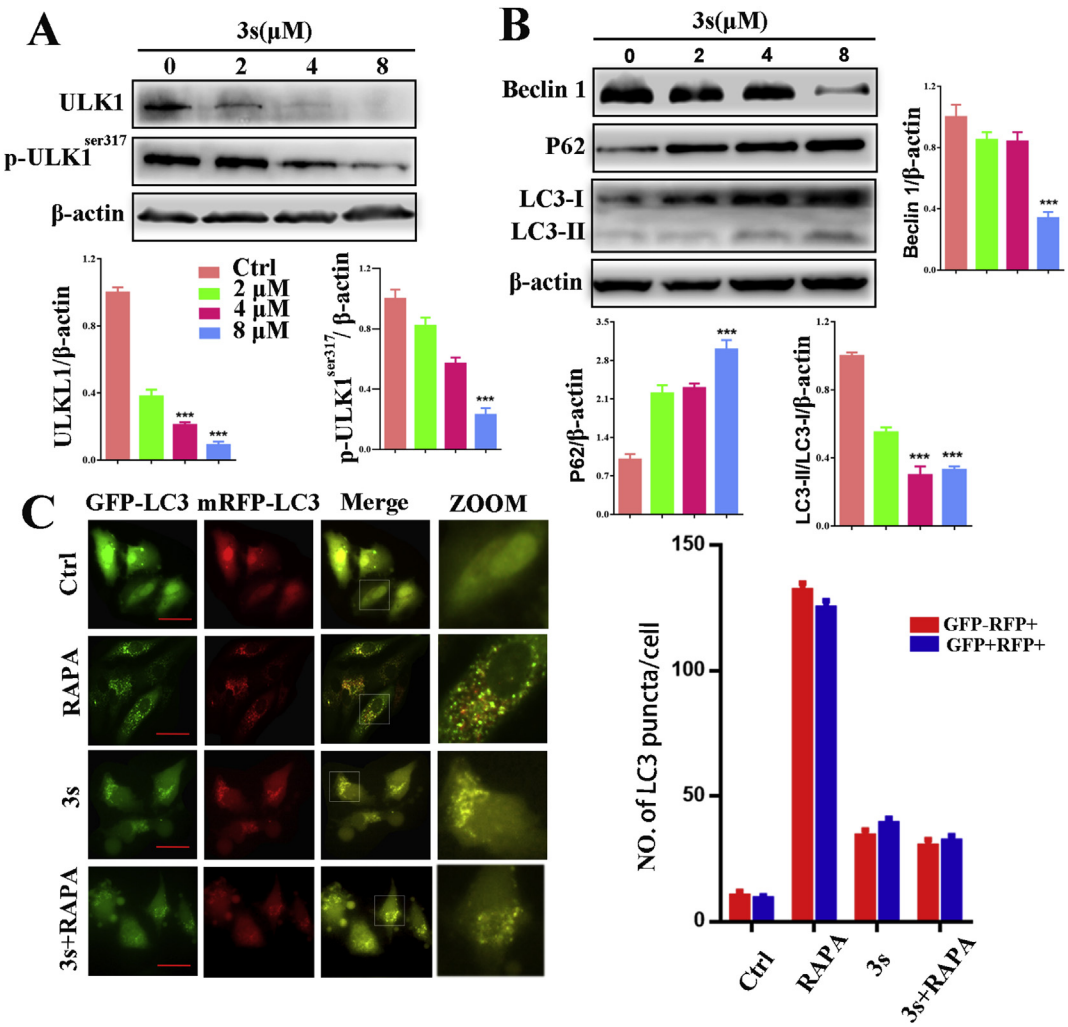


**Fig. 5. Compound 3s inhibits autophagy via the ULK3s blocks autophagy by ULK1 inhibition in A549 cells.** (A) A549 cells were treated with control or **3s** for 24 h, and then the expression of ULK1, *p*-ULK1 (ser317) was detected by Western blot analysis. (B) The expression levels of p62, Beclin 1 and LC3I/II were determined by Western blot analysis. (C) The expression of LC3B puncta was observed by fluorescence microscope. Blue: DAPI. Scale bar: 10 μm. (For interpretation of the references to color in this figure legend, the reader is referred to the Web version of this article.)

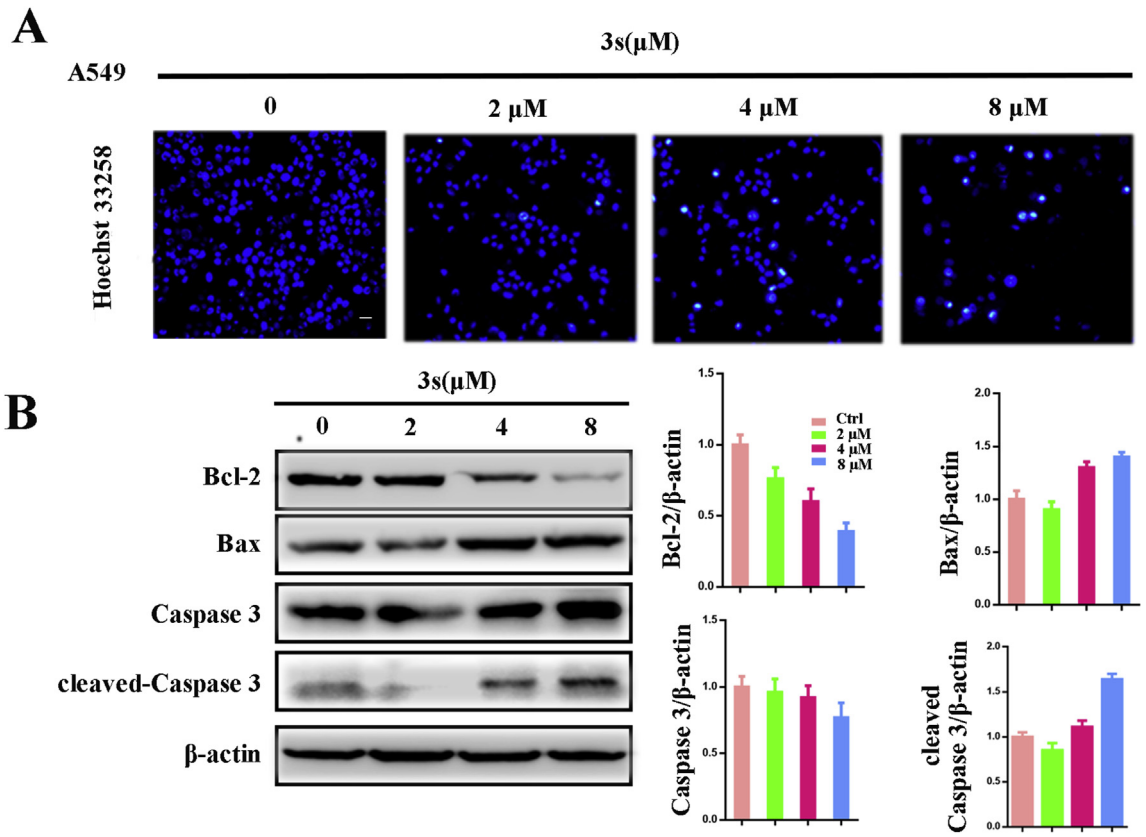


**Fig. 6. 3s promotes apoptosis in A549 cells.** (A) After treatment with Compound **3s**, A549 cells were stained with Hoechst 33258. Scale bar: 20 μm. (B) After **3s** treatment, the expression levels of Bax, Bcl-2, cleaved-Caspase 3 and Caspase3 were determined by Western blot analysis.

Moreover, we further demonstrate that compound **3s** can suppress cytoprotective autophagy and promote apoptosis in NSCLC cells. Taken together, these findings shed new light on compound **3s** that would be further utilized as a promising candidate drug for the future NSCLC therapy.

## 4. Experimental section

### 4.1. Cell culture and reagent

All the cell lines used in this study were purchased from American Type Culture Collection (ATCC, Manassas, VA, USA). A549, MDA-MB-468 and MCF-7 cells were cultured in Dulbecco Modified Eagle Medium (DMEM) supplemented with 10% fetal bovine serum and incubated with 5% $CO_2$. HL60 and U937 cells were cultured in RPMI 1640 culture medium supplemented with 10% fetal bovine serum. MTT (#M2128) was purchased from Sigma-Aldrich (St. Louis, MO, USA). Primary antibodies against ULK1 (#8054), *p*-ULK1ser317 (#12753), p62 (#8025), Beclin 1 (#3495), *p*-Beclin1ser15 (#84966), Bax (#5023), Bcl-2 (#2870), Caspase-3 (#9662), Atg13 (#13468), *p*-Atg13ser318 (#46329) were purchased from Cell Signaling Technologies (Boston, MA, USA). Rapamycin (#ab120224) was purchased from Abcam (Cambridge, UK). GFP/mRFP-LC3 (HB-AP2100001) was purchased from HANBIO (China). ADP-Glo™ Kinase Assay (#V9101) and ULK1 Kinase Enzyme System (#V3521) were purchase from Promega (Madison, WI, USA).

### 4.2. Cell viability assay

Cells were dispensed in 96-well plates at a density of $5.5 \times 10^4$ cells/mL. After 24 h incubation, cells were treated with different concentrations of synthetic compounds for the indicated time periods. Cell viability was measured by the MTT assay.

### 4.3. Molecular docking and pharmacophore modeling

Discovery Studio software (version 3.1) was used to run all the calculations [30]. Docking program adopts the CHARMm force field to minimize energy of the ligands. The crystal structure of the ULK1 kinase (PDB code: 4WNO) was taken from PDB database. The binding sphere was primarily defined within 10 Å from its original ligand. Gold score was selected as the scoring function. Identification of the critical pharmacophoric features is important for potent ULK1 inhibitors. All the training set molecules were subjected to find the common chemical features of reported ULK1 inhibitors. Hydrogen bond acceptor, hydrogen bond donor, ring aromatic and hydrophobic aromatic chemical features were selected with the parameters of minimum "0" to maximum of "5". Ten quantitative pharmacophore models were generated with corresponding statistical parameters such as cost values, root mean square and fit values. The best quality hypothesis was selected. Images were created using PyMOL.

### 4.4. Hoechst 33258 staining

Cells ($1 \times 10^5$ per well) were treated Compound **3s** or rapamycin together with Compound **3s** for 24 h. After washed twice with cold PBS, the cells were stained with Hoechst 33258 in the dark at 37 C for 30 min. Then the morphological change of cell was observed under fluorescence microscope.

### 4.5. *GFP/mRFP - LC3 transfection*

The method was as previous description [31,32]. The A549 cells were sequentially incubated, starting with GFP/mRFP-LC3 transfected for 6 h. Then the transfected cells were used for subsequent experiments 24 h later and were analyzed under a fluorescence microscope.

### 4.6. Flow cytometric analysis

For Annexin V-FITC/PI staining, the treated cells were collected, washed twice with PBS and then stained with Annexin V-FITC (1:1000) in binding buffer at room temperature in the dark. 15 min later, the cells were incubated with PI staining solution for 5 min. Then the cells were measured by flow cytometry (Becton Dickinson).

### 4.7. Western blot analysis

Western blot analysis was carried out by the method as previous description [33]. Cells were treated with Compound **3s** and SBI0206965 for indicated times. Then both adherent and floating cells were collected, which was added with a Rapa Buffer with Protease Inhibitor and Phosphatase inhibitor Cocktail (Sigma-Aldrich) after centrifugation (12,000 g at 4 °C for 15 min); the protein concentration was determined using the BCA method. Proteins were separated by sodium dodecyl sulphate-polyacrylamide gel electrophoresis and transferred to nitrocellulose membranes. The membranes were blocked with Tris Buffered Saline with Tween-20 (TBST) containing 5% skimmed milk at room temperature for 1 h, incubated overnight with primary antibodies at 4 °C and subsequently incubated with secondary horseradish peroxidaseconjugated, goat anti-rabbit or goat anti-mouse IgG (Abcam) at room temperature for 1 h, then visualized by using ECL reagents.

### 4.8. In vitro kinase activity assays

Kinase inhibitor specificity profiling assays were first carried out using the Kinase Profiler service of Eurofins Pharma Discovery Services UK Limited according to the protocols described below (for details on more kinases, see http://www.eurofins.com/pharmadiscovery). The concentration of the compound in each assay was 10 μM.

ULK1 kinase activity assay was performed using ADP-Glo™ Kinase Assay. The ADP-Glo™ Kinase Assay is a luminescent kinase assay that measures ADP formed from a kinase reaction; ADP is converted into ATP, which is converted into light by Ultra-Glo™ Luciferase. The luminescent signal positively correlates with kinase activity. The kinase reaction is performed by kinase buffer (40 mM Tris pH 7.5; 20 mM $MgCl_2$; 0.1 mg/ml BSA; 50 mM DTT). The ULK1 kinase enzyme, substrate, compound, DMSO, and ATP were diluted in kinase buffer. Then, 1 μl compound or DMSO, 2 μl ULK1 kinase (10 ng), or 2 μl ATP (10 μM)/mixMBP (0.1 μg/μl) were added to the wells of a 384-well plate. The plate was mixed and incubated at room temperature for 60 min. After the kinase reaction incubation, 5 μl of ADP-Glo™ reagent was added per well. Then the plates were mixed for 2 min and incubated at room temperature for 40 min 10 μl of kinase detection reagent was added to all the wells and incubated at room temperature for 30 min. The luminescence was measured.

### 4.9. Statistical analysis

All the presented data and results were confirmed in at least 3 independent experiments. The data are expressed as means ± SD and analyzed with GraphPad Prism 6.0. Statistical comparisons were made by 1-way ANOVA and Student's *t*-test of SPSS 17.0 (Chicago, IL, USA). $P < 0.05$ was considered statistically significant.

### 4.10. General procedure for the synthesis of compounds ***3a-3u, 5a, 8a-c, 10a-b***

To a solution of 2-hydroxybenzoic acid (30.0 mmol), and EDCI (30.0 mmol) in ethyl acetate (250 mL) was added methylamine (150.0 mmol) after stirring for 10 min at room temperature. The reaction was allowed to r.t. for overnight. After completion, the solvent was removed under reduced pressure to give the crude product. The crude product was purified by silica gel flash chromatography (petroleum ether/ethyl acetate 5:1) to afforded intermediate **1a**. A 100 ml round bottom flask was charged with 50 ml ethanol at 0 °C. After 15 min, the intermediate 1, 5-bromo-2,4-dichloropyrimidine and DIEA were added dropwise at 0 °C, and removed to room temperature for additional 8 h. Upon completion, the residue was concentrated to give the crude oil. Intermediate **2a** was purified by silica gel flash chromatography (petroleum ether/ethyl acetate 3:1) as a colorless oil. The mixture of **2a** (0.5 mmol, 1 eq), 3,4,5-trimethoxyaniline (0.6 mmol, 1.2 eq) and *p*-TsA (0.1 mmol, 0.2 eq) in THF was stirred at 80 °C overnight. After the completion of the reaction, the crude product was purified by silica gel using PE/EA (3:1) to produce **3a**. The procedure was also applied to the following compounds **3b-u**, **5a**. To a solution of 2,4-dichloropyrimidine (10 mmol), *N*-Boc-1,3-propanediamine (10 mmol) and $K_2CO_3$ (20 mmol) were stirred in isopropanol and heated at 80 °C for 24 h. After the completion of the reaction, the filtration was processed to give intermediate **6a**. The mixture of **6a** (1 mmol, 1 eq), 3,4,5-trimethoxyaniline (1.2 mmol, 1.2 eq) and *p*-TsA (0.2 mmol, 0.2 eq) in THF was stirred at 80 °C overnight. The reaction mixture was subsequently evaporated, and the residue was purified by chromatography (petroleum ether/ethyl acetate = 4:1) to **7a**. The *N*-Boc group was removed by TFA in $CH_2Cl_2$ to provide the final compound **8a**. Similarly, **10a-b** were yielded by **9a-b** with N, *N*′-diethyl-ethylenediamine.

#### 4.10.1. Preparation of 2-((5-bromo-2-((4-bromophenyl)amino) pyrimidin-4-yl)oxy)-N-methylbenzamide (***3a***)

*4.10.1.1. 2-((5-Bromo-2-((4-bromophenyl)amino)pyrimidin-4-yl) oxy)-N-methylbenzamide (**3a**).* White powder; Yield 82%; m.p. 212–215 °C; $^1$H NMR (400 MHz, DMSO-$d_6$) δ 9.81 (s, 1H), 8.52 (s, 1H), 8.13 (d, $J$ = 4.4 Hz, 1H), 7.66 (d, $J$ = 7.6 Hz, 1H), 7.61 (t, $J$ = 7.6 Hz, 1H), 7.45 (t, $J$ = 7.5 Hz, 1H), 7.37 (d, $J$ = 8.0 Hz, 1H), 7.29 (d, $J$ = 7.9 Hz, 2H), 7.17 (d, $J$ = 8.5 Hz, 2H), 2.64 (d, $J$ = 4.6 Hz, 3H); $^{13}$C NMR (100 MHz, DMSO-$d_6$) δ 165.84, 165.50, 160.66, 158.15, 150.05, 139.60, 131.80, 131.32 (2C), 130.10, 129.55, 126.54, 124.33, 120.99 (2C), 113.46, 93.44, 26.50; HRMS: calcd. for $C_{18}H_{14}Br_2N_4O_2$: 498.9381 $[M+Na]^+$, found: 498.9381.

*4.10.1.2. 2-((5-Bromo-2-((4-(trifluoromethyl)phenyl)amino)pyrimidin-4-yl)oxy)-N-methylbenzamide (**3b**).* White powder; Yield 72%; m.p. 229–234 °C; $^1$H NMR (400 MHz, DMSO-$d_6$) δ 10.08 (s, 1H), 8.58 (s, 1H), 8.16 (d, $J$ = 4.5 Hz, 1H), 7.67 (dd, $J$ = 7.7, 1.5 Hz, 1H), 7.64 (td, $J$ = 7.6, 1.2 Hz, 1H), 7.52 (d, $J$ = 8.2 Hz, 2H), 7.46 (td, $J$ = 7.6, 0.8 Hz, 1H), 7.39 (d, $J$ = 8.1 Hz, 1H), 7.35 (d, $J$ = 8.6 Hz, 2H), 2.64 (d, $J$ = 4.6 Hz, 3H); $^{13}$C NMR (100 MHz, DMSO-$d_6$) δ 165.85, 165.61, 160.73, 158.06, 150.06, 143.87, 131.83, 130.12, 129.57, 126.58, 126.33, 125.80, 124.33, 123.65, 121.80, 118.72 (2C), 94.29, 26.49; HRMS: calcd. for $C_{19}H_{14}BrF_3N_4O_2$: 489.0150 $[M+Na]^+$, found: 489.0151.

*4.10.1.3. 2-((5-Bromo-2-((2-fluorophenyl)amino)pyrimidin-4-yl) oxy)-N-methylbenzamide (**3c**).* White solid; Yield 79%; m.p.

150–152 °C; $^1$H NMR (400 MHz, DMSO-$d_6$) δ 9.12 (s, 1H), 8.45 (s, 1H), 8.09 (d, $J$ = 4.5 Hz, 1H), 7.59 (dd, $J$ = 7.5, 1.3 Hz, 1H), 7.53 (td, $J$ = 7.8, 1.5 Hz, 1H), 7.42 (td, $J$ = 8.1, 1.0 Hz, 1H), 7.39–7.30 (m, 2H), 7.18–7.08 (m, 1H), 7.03 (dd, $J$ = 12.9, 6.2 Hz, 1H), 6.90 (t, $J$ = 7.6 Hz, 1H), 2.65 (d, $J$ = 4.6 Hz, 3H); $^{13}$C NMR (100 MHz, DMSO-$d_6$) δ 166.08, 165.15, 160.65, 158.89, 156.13, 153.69, 149.71, 131.52, 130.15, 129.34, 127.21, 126.30, 125.20, 124.26, 124.04, 115.75, 93.73, 26.49; HRMS: calcd. for $C_{18}H_{14}BrFN_4O_2$: 439.0182 [M+Na]$^+$, found: 439.0181.

*4.10.1.4. 2-((5-Bromo-2-((3-bromophenyl)amino)pyrimidin-4-yl) oxy)-N-methylbenzamide (**3d**).* White solid; Yield 75%; m.p. 209–214 °C; $^1$H NMR (400 MHz, DMSO-$d_6$) δ 9.81 (s, 1H), 8.55 (s, 1H), 8.11 (d, $J$ = 4.6 Hz, 1H), 7.63 (dd, $J$ = 7.6, 1.5 Hz, 2H), 7.60 (td, $J$ = 7.8, 1.6 Hz, 1H), 7.41 (td, $J$ = 7.9, 1.3 Hz, 1H), 7.38 (d, $J$ = 8.1 Hz, 1H), 7.32 (d, $J$ = 7.5 Hz, 1H), 7.07–6.93 (m, 2H), 2.64 (d, $J$ = 4.6 Hz, 3H); $^{13}$C NMR (100 MHz, DMSO-$d_6$) δ 165.91, 165.44, 160.62, 158.18, 149.88, 141.84, 131.92, 130.56, 129.93, 129.54, 126.65, 124.64, 124.04, 121.86, 121.16, 117.95, 93.96, 26.50; HRMS: calcd. for $C_{18}H_{14}Br_2N_4O_2^+$: 498.9381 [M+Na]$^+$, found: 498.9379.

*4.10.1.5. 2-((5-Bromo-2-((2-methoxyphenyl)amino)pyrimidin-4-yl) oxy)-N-methylbenzamide (**3e**).* White solid; Yield 68%; m.p. 158–160 °C; $^1$H NMR (400 MHz, DMSO-$d_6$) δ 8.47 (s, 1H), 8.12 (d, $J$ = 4.5 Hz, 1H), 8.07 (s, 1H), 7.62 (dd, $J$ = 7.6, 1.5 Hz, 1H), 7.57 (td, $J$ = 7.8, 1.6 Hz, 1H), 7.50 (d, $J$ = 7.8 Hz, 1H), 7.40 (td, $J$ = 7.5, 0.9 Hz, 1H), 7.36 (d, $J$ = 8.1 Hz, 1H), 7.02–6.88 (m, 2H), 6.62 (t, $J$ = 5.7 Hz, 1H), 3.78 (s, 3H), 2.64 (d, $J$ = 4.6 Hz, 3H); $^{13}$C NMR (100 MHz, DMSO-$d_6$) δ 166.06, 165.25, 160.64, 158.43, 149.81, 149.63, 131.58, 130.16, 129.40, 128.08, 126.38, 124.11, 123.61, 121.06, 120.47, 111.18, 93.36, 56.13, 26.48; HRMS: calcd. for $C_{19}H_{17}BrN_4O_3$: 451.0382 [M+Na]$^+$, found: 451.0378.

*4.10.1.6. 2-((5-Bromo-2-(m-tolylamino)pyrimidin-4-yl)oxy)-N-methylbenzamide (**3f**).* White solid; Yield 77%; m.p. 183–186 °C; $^1$H NMR (400 MHz, DMSO-$d_6$) δ 9.58 (s, 1H), 8.49 (s, 1H), 8.09 (d, $J$ = 4.5 Hz, 1H), 7.64 (d, $J$ = 7.6 Hz, 1H), 7.59 (td, $J$ = 7.9, 1.4 Hz, 1H), 7.41 (t, $J$ = 7.7 Hz, 1H), 7.37 (d, $J$ = 8.1 Hz, 1H), 7.19 (s, 1H), 7.09 (d, $J$ = 7.5 Hz, 1H), 6.92 (t, $J$ = 7.8 Hz, 1H), 6.66 (d, $J$ = 7.4 Hz, 1H), 2.64 (d, $J$ = 4.6 Hz, 3H), 2.07 (s, 3H); $^{13}$C NMR (100 MHz, DMSO-$d_6$) δ 165.90, 165.30, 160.57, 158.54, 150.03, 140.02, 137.90, 131.73, 130.09, 129.49, 128.49, 126.44, 124.22, 122.86, 119.52, 116.53, 92.85, 26.51, 21.83; HRMS: calcd. for $C_{19}H_{17}BrN_4O_2$: 435.0433 [M+Na]$^+$, found: 435.0435.

*4.10.1.7. 2-((5-Bromo-2-((2,4-dimethylphenyl)amino)pyrimidin-4-yl)oxy)-N-methylbenzamide (**3g**).* White powder; Yield 70%; m.p. 109–113 °C; $^1$H NMR (400 MHz, DMSO-$d_6$) δ 8.66 (s, 1H), 8.34 (s, 1H), 8.01 (d, $J$ = 4.5 Hz, 1H), 7.57 (dd, $J$ = 7.5, 1.4 Hz, 1H), 7.50 (td, $J$ = 7.8, 1.6 Hz, 1H), 7.39–7.27 (m, 2H), 7.09 (d, $J$ = 8.1 Hz, 1H), 6.91 (s, 1H), 6.77 (d, $J$ = 7.9 Hz, 1H), 2.66 (d, $J$ = 4.6 Hz, 3H), 2.19 (s, 3H), 2.07 (s, 3H); $^{13}$C NMR (100 MHz, DMSO-$d_6$) δ 166.18, 164.87, 160.54, 159.82, 149.74, 135.03, 133.93, 132.24, 131.46, 131.07, 130.16, 129.28, 126.62, 126.09, 125.33, 123.89, 92.52, 26.55, 20.93, 18.35; HRMS: calcd. for $C_{20}H_{19}BrN_4O_2$: 449.0589 [M+Na]$^+$, found: 449.0591.

*4.10.1.8. 2-((5-Bromo-2-((4-chloro-2-fluorophenyl)amino)pyrimidin-4-yl)oxy)-N-methylbenzamide (**3h**).* White powder; Yield 88%; m.p. 157–159 °C; $^1$H NMR (400 MHz, DMSO-$d_6$) δ 9.27 (s, 1H), 8.48 (s, 1H), 8.12 (d, $J$ = 4.6 Hz, 1H), 7.60 (dd, $J$ = 7.6, 1.3 Hz, 1H), 7.55 (td, $J$ = 7.9, 1.5 Hz, 1H), 7.45 (t, $J$ = 8.8 Hz, 1H), 7.39 (d, $J$ = 7.5 Hz, 1H), 7.37–7.31 (m, 2H), 6.94 (d, $J$ = 8.1 Hz, 1H), 2.64 (d, $J$ = 4.6 Hz, 3H); $^{13}$C NMR (100 MHz, DMSO-$d_6$) δ 166.03, 165.28, 160.70, 158.59, 155.77, 149.71, 131.60, 130.12, 129.39, 126.65, 126.54, 126.39, 125.81, 124.27, 124.05, 116.37, 94.12, 26.48; HRMS: calcd. for $C_{18}H_{13}BrClFN_4O_2$: 472.9792 [M+Na]$^+$, found: 472.9790.

*4.10.1.9. 2-((5-Bromo-2-((3-(trifluoromethyl)phenyl)amino)pyrimidin-4-yl)oxy)-N-methylbenzamide (**3i**).* White solid; Yield 72%; m.p. 200–203 °C; $^1$H NMR (400 MHz, DMSO-$d_6$) δ 9.95 (s, 1H), 8.57 (s, 1H), 8.12 (d, $J$ = 4.4 Hz, 1H), 7.76 (s, 1H), 7.69–7.61 (m, 2H), 7.57 (td, $J$ = 7.9, 1.5 Hz, 1H), 7.40 (dd, $J$ = 15.3, 7.8 Hz, 2H), 7.24 (t, $J$ = 7.8 Hz, 1H), 7.19 (d, $J$ = 7.6 Hz, 1H), 2.64 (d, $J$ = 4.6 Hz, 3H); $^{13}$C NMR (100 MHz, DMSO-$d_6$) δ 165.90, 165.46, 160.65, 158.23, 149.89, 131.75, 129.99, 129.78, 129.71, 129.49, 126.50, 125.89, 124.03, 123.18, 122.64, 118.25, 115.17, 94.25, 26.49; HRMS: calcd. for $C_{19}H_{14}BrF_3N_4O_2$: 489.0150 [M+Na]$^+$, found: 489.0151.

*4.10.1.10. 2-((5-Bromo-2-((3-methoxyphenyl)amino)pyrimidin-4-yl) oxy)-N-methylbenzamide (**3j**).* Yellow solid; Yield 62%; m.p. 136–139 °C; $^1$H NMR (400 MHz, DMSO-$d_6$) δ 9.94 (d, $J$ = 12.5 Hz, 1H), 9.85 (s, 1H), 8.59 (s, 1H), 7.28 (s, 1H), 7.22 (dd, $J$ = 15.4, 7.6 Hz, 2H), 7.15 (t, $J$ = 8.1 Hz, 1H), 7.06 (d, $J$ = 7.7 Hz, 1H), 6.79 (t, $J$ = 7.5 Hz, 2H), 6.55 (dd, $J$ = 8.0, 1.7 Hz, 1H), 3.72 (s, 3H), 3.28 (s, 3H); $^{13}$C NMR (100 MHz, DMSO-$d_6$) δ 169.13, 161.82, 161.44, 159.95, 159.00, 155.24, 141.19, 132.14, 129.76, 129.65, 122.77, 119.09, 116.55, 112.00, 107.75, 105.47, 104.58, 55.40, 35.75; HRMS: calcd. for $C_{19}H_{17}BrN_4O_3$: 451.0382 [M+Na]$^+$, found: 451.0376.

*4.10.1.11. 2-((5-Bromo-2-((3-isopropylphenyl)amino)pyrimidin-4-yl) oxy)-N-methylbenzamide (**3k**).* White powder; Yield 93%; m.p. 135–137 °C; $^1$H NMR (400 MHz, DMSO-$d_6$) δ 9.55 (s, 1H), 8.49 (s, 1H), 8.08 (d, $J$ = 3.6 Hz, 1H), 7.63 (d, $J$ = 7.6 Hz, 1H), 7.58 (t, $J$ = 7.6 Hz, 1H), 7.39 (dd, $J$ = 17.3, 7.9 Hz, 2H), 7.22 (s, 1H), 7.17 (d, $J$ = 5.4 Hz, 1H), 6.94 (t, $J$ = 7.6 Hz, 1H), 6.74 (d, $J$ = 7.5 Hz, 1H), 2.65 (d, $J$ = 4.4 Hz, 3H), 2.59 (dd, $J$ = 13.3, 6.7 Hz, 1H), 1.08 (d, $J$ = 6.8 Hz, 6H); $^{13}$C NMR (100 MHz, DMSO-$d_6$) δ 165.91, 165.25, 160.55, 158.58, 150.03, 149.09, 139.99, 131.69, 130.07, 129.48, 128.59, 126.38, 124.14, 119.79, 117.56, 116.90, 92.92, 33.89, 26.51, 24.36 (2C); HRMS: calcd. for $C_{21}H_{21}BrN_4O_2$: 463.0746 [M+Na]$^+$, found: 463.0745.

*4.10.1.12. 2-((2-(benzo[d] [1,3]dioxol-5-ylamino)-5-bromopyrimidin-4-yl)oxy)-N-methylbenzamide (**3l**).* Yellow solid; Yield 85%; m.p. 182–184 °C; $^1$H NMR (400 MHz, DMSO-$d_6$) δ 9.91 (s, 1H), 9.72 (s, 1H), 8.54 (s, 1H), 7.26–7.17 (m, 2H), 7.10 (s, 1H), 6.90–6.71 (m, 4H), 5.96 (s, 2H), 3.26 (s, 3H); $^{13}$C NMR (100 MHz, DMSO-$d_6$) δ 169.11, 161.82, 161.48, 158.98, 155.21, 147.44, 142.72, 134.28, 132.11, 129.68, 122.79, 119.14, 116.55, 112.61, 108.33, 103.83, 102.11, 101.30, 35.69; HRMS: calcd. for $C_{19}H_{15}BrN_4O_4$: 465.0174 [M+Na]$^+$, found: 465.0178.

*4.10.1.13. 5-Bromo-4-(2-ethoxyphenoxy)-N-(m-tolyl)pyrimidin-2-amine (**3m**).* White solid; Yield 81%; m.p. 100–103 °C; $^1$H NMR (400 MHz, DMSO-$d_6$) δ 9.64 (s, 1H), 8.50 (s, 1H), 7.31 (dd, $J$ = 12.3, 4.8 Hz, 1H), 7.27 (dd, $J$ = 7.9, 1.3 Hz, 1H), 7.23–7.14 (m, 2H), 7.05 (dd, $J$ = 15.5, 7.8 Hz, 2H), 6.91 (t, $J$ = 7.8 Hz, 1H), 6.65 (d, $J$ = 7.4 Hz, 1H), 3.97 (q, $J$ = 6.9 Hz, 2H), 2.05 (s, 3H), 1.05 (t, $J$ = 6.9 Hz, 3H); $^{13}$C NMR (100 MHz, DMSO-$d_6$) δ 165.08, 160.63, 158.70, 150.60, 142.05, 140.12, 137.94, 128.50, 127.43, 123.28, 122.77, 121.48, 119.23, 116.26, 115.09, 92.36, 64.54, 21.82, 14.90; HRMS: calcd. for $C_{19}H_{18}BrN_3O_2$: 422.0480 [M+*Na*]$^+$, found: 422.0480.

*4.10.1.14. 5-Bromo-4-(3-fluorophenoxy)-N-(m-tolyl)pyrimidin-2-amine (**3n**).* White solid; Yield 68%; m.p. 125–127 °C; $^1$H NMR (400 MHz, DMSO-$d_6$) δ 9.73 (s, 1H), 8.54 (s, 1H), 7.54 (dd, $J$ = 15.1, 8.2 Hz, 1H), 7.33 (dt, $J$ = 9.9, 2.2 Hz, 1H), 7.23 (s, 1H), 7.21 (dd, $J$ = 8.8, 2.1 Hz, 1H), 7.17 (dd, $J$ = 8.2, 1.7 Hz, 1H), 7.12 (d, $J$ = 7.7 Hz, 1H), 6.96 (t, $J$ = 7.8 Hz, 1H), 6.69 (d, $J$ = 7.4 Hz, 1H), 2.08 (s, 3H); $^{13}$C NMR (100 MHz, DMSO-$d_6$) δ 164.95, 162.96 (d, $J$ = 245.0 Hz), 161.09, 158.62, 153.74, 139.96, 137.94, 131.49, 128.50, 123.04, 119.54, 118.79, 116.62, 113.38, 110.69, 92.64, 21.67; HRMS: calcd. for $C_{17}H_{13}BrFN_3O$: 374.0304 [M+H]$^+$, found: 374.0306.

*4.10.1.15. 5-Bromo-4-(3,5-dichlorophenoxy)-N-(m-tolyl)pyrimidin-2-amine (**3o**).* White solid; Yield 82%; m.p. 163–165 °C; $^1$H NMR (400 MHz, DMSO-$d_6$) δ 9.78 (s, 1H), 8.55 (s, 1H), 7.64 (s, 1H), 7.57 (s, 2H), 7.20 (s, 1H), 7.15 (d, $J$ = 7.5 Hz, 1H), 7.00 (t, $J$ = 7.7 Hz, 1H), 6.72 (d, $J$ = 7.3 Hz, 1H), 2.11 (s, 3H); $^{13}$C NMR (100 MHz, DMSO-$d_6$) δ 164.79, 161.25, 158.53, 153.93, 139.92, 137.96, 135.06 (2C), 128.53, 126.45, 123.16, 122.32 (2C), 119.60, 116.65, 92.54, 21.59; HRMS: calcd. for $C_{17}H_{12}BrCl_2N_3O$: 423.9619 $[M+H]^+$, found: 423.9614.

*4.10.1.16. 5-Bromo-4-(3-nitrophenoxy)-N-(m-tolyl)pyrimidin-2-amine (**3p**).* White solid; Yield 77%; m.p. 164–166 °C; $^1$H NMR (400 MHz, DMSO-$d_6$) δ 9.74 (s, 1H), 8.57 (s, 1H), 8.31–8.18 (m, 2H), 7.89–7.76 (m, 2H), 7.14 (s, 1H), 7.08 (d, $J$ = 7.0 Hz, 1H), 6.91 (t, $J$ = 7.7 Hz, 1H), 6.67 (d, $J$ = 7.3 Hz, 1H), 2.02 (s, 3H); $^{13}$C NMR (100 MHz, DMSO-$d_6$) δ 164.83, 161.28, 158.50, 153.07, 149.01, 139.83, 137.86, 131.62, 129.75, 128.43, 123.15, 121.35, 119.63, 118.26, 116.70, 92.68, 21.58; HRMS: calcd. for $C_{17}H_{13}BrN_4O_3$: 401.0249 $[M+H]^+$, found: 401.0248.

*4.10.1.17. 5-Bromo-4-(4-bromophenoxy)-N-(m-tolyl)pyrimidin-2-amine (**3q**).* Yellow solid; Yield 91%; m.p. 186–188 °C; $^1$H NMR (400 MHz, DMSO-$d_6$) δ 9.72 (s, 1H), 8.53 (s, 1H), 7.69 (d, $J$ = 8.8 Hz, 2H), 7.29 (d, $J$ = 8.8 Hz, 2H), 7.22 (s, 1H), 7.07 (d, $J$ = 6.9 Hz, 1H), 6.97 (t, $J$ = 7.8 Hz, 1H), 6.69 (d, $J$ = 7.3 Hz, 1H), 2.08 (s, 3H); $^{13}$C NMR (100 MHz, DMSO-$d_6$) δ 165.06, 161.05, 158.56, 152.06, 139.96, 137.99, 133.16 (2C), 128.48, 125.01 (2C), 123.01, 119.43, 118.86, 116.59, 92.59, 21.74; HRMS: calcd. for $C_{17}H_{13}Br_2N_3O$: 433.9504 $[M+H]^+$, found: 433.9502.

*4.10.1.18. 4-(4-(benzyloxy)phenoxy)-5-bromo-N-(m-tolyl)pyrimidin-2-amine (**3r**).* White solid; Yield 65%; m.p. 178–180 °C; $^1$H NMR (400 MHz, DMSO-$d_6$) δ 9.67 (s, 1H), 8.50 (s, 1H), 7.49 (d, $J$ = 7.1 Hz, 2H), 7.43 (t, $J$ = 7.2 Hz, 2H), 7.40–7.32 (m, 1H), 7.29–7.17 (m, 3H), 7.12 (d, $J$ = 8.7 Hz, 3H), 6.91 (t, $J$ = 7.6 Hz, 1H), 6.67 (d, $J$ = 7.0 Hz, 1H), 5.13 (s, 2H), 2.07 (s, 3H); $^{13}$C NMR (100 MHz, DMSO-$d_6$) δ 165.51, 160.74, 158.66, 156.61, 146.19, 140.06, 137.97, 137.45, 128.97 (2C), 128.50, 128.41, 128.24 (2C), 123.42 (2C), 122.87, 119.35, 116.49, 116.03 (2C), 92.66, 70.09, 21.74; HRMS: calcd. for $C_{24}H_{20}BrN_3O_2$: 462.0817 $[M+H]^+$, found: 462.0815.

*4.10.1.19. 5-Bromo-4-(2-fluoro-4-nitrophenoxy)-N-(3,4,5-trimethoxyphenyl)pyrimidin-2-amine (**3s**).* Yellow powder; Yield 87%; m.p. 190–193 °C; $^1$H NMR (400 MHz, DMSO-$d_6$) δ 9.68 (s, 1H), 8.63 (s, 1H), 8.42 (d, $J$ = 8.6 Hz, 1H), 8.23 (d, $J$ = 8.5 Hz, 1H), 7.84 (t, $J$ = 8.3 Hz, 1H), 6.78 (s, 2H), 3.56 (s, 6H), 3.55 (s, 3H); $^{13}$C NMR (100 MHz, DMSO-$d_6$) δ 163.74, 161.74, 158.59, 153.53, 153.06 (2C), 145.98, 145.30, 135.68, 133.93, 125.59, 121.51, 113.65, 98.62 (2C), 92.22, 60.57, 56.36 (2C); HRMS: calcd. for $C_{19}H_{16}BrFN_4O_6$: 517.0135 $[M+Na]^+$, found: 517.0135.

*4.10.1.20. 5-Bromo-N-(4-chlorophenyl)-4-(2-fluoro-4-nitrophenoxy)pyrimidin-2-amine (**3t**).* Yellow powder; Yield 70%; m.p. 175–178 °C; $^1$H NMR (400 MHz, DMSO-$d_6$) δ 10.01 (s, 1H), 8.66 (s, 1H), 8.48 (d, $J$ = 8.6 Hz, 1H), 8.27 (d, $J$ = 8.3 Hz, 1H), 7.84 (t, $J$ = 8.2 Hz, 1H), 7.35 (s, 2H), 7.14 (d, $J$ = 7.5 Hz, 2H); $^{13}$C NMR (100 MHz, DMSO-$d_6$) δ 163.96, 161.87, 158.26, 153.71, 146.30, 145.20, 138.75, 128.61 (2C), 126.22, 125.95, 121.57, 120.93 (2C), 113.67, 92.53; HRMS: calcd. for $C_{16}H_9BClFN_4O_3$: 438.9609 $[M+H]^+$, found: 438.9606.

*4.10.1.21. 5-Bromo-N-(4-bromophenyl)-4-(2-fluoro-4-nitrophenoxy)pyrimidin-2-amine (**3u**).* Yellow powder; Yield 76%; m.p. 163–165 °C; $^1$H NMR (400 MHz, DMSO-$d_6$) δ 10.01 (s, 1H), 8.66 (s, 1H), 8.48 (dd, $J$ = 10.1, 2.5 Hz, 1H), 8.26 (dd, $J$ = 8.9, 1.4 Hz, 1H), 7.94–7.75 (m, 1H), 7.27 (t, $J$ = 9.7 Hz, 4H); $^{13}$C NMR (100 MHz, DMSO-$d_6$) δ 163.96, 161.86, 158.22, 153.71, 146.30, 145.20, 139.17, 131.50 (2C), 125.95, 121.56, 121.32 (2C), 114.17, 113.67, 92.58; HRMS: calcd. for $C_{16}H_9Br_2FN_4O_3$: 482.9104 $[M+H]^+$, found: 482.9103.

*4.10.1.22. 4-(2-Fluoro-4-nitrophenoxy)-N-(3,4,5-trimethoxyphenyl)pyrimidin-2-amine (**5a**).* White solid; Yield 58%; m.p. 156–158 °C; $^1$H NMR (400 MHz, DMSO-$d_6$) δ 9.67 (s, 1H), 8.63 (s, 1H), 8.41 (dd, $J$ = 10.1, 2.6 Hz, 1H), 8.23 (dd, $J$ = 9.0, 2.7 Hz, 1H), 7.91–7.78 (m, 1H), 6.79 (s, 2H), 3.57 (s, 3H), 3.56 (s, 3H), 3.32 (s, 3H). $^{13}$C NMR (100 MHz, DMSO-$d_6$) δ 163.73, 161.73, 158.58, 154.77, 153.04 (2C), 152.27, 145.93, 145.22, 135.65, 133.97, 125.57, 121.48, 113.74, 98.67, 92.20, 60.56, 56.37 (2C). HRMS: calcd. for $C_{19}H_{17}FN_4O_6$: 417.1205 $[M+H]^+$, found: 417.1205.

*4.10.1.23. $N^4$-(3-aminopropyl)-5-bromo-$N^2$-(3,4,5-trimethoxyphenyl)pyrimidine-2,4-diamine (**8a**).* Yellow powder; Yield 70%; m.p. 123–125 °C; $^1$H NMR (400 MHz, DMSO-$d_6$) δ8.14 (s, 1H), 7.68 (s, 1H), 7.10 (s, 2H), 6.98 (s, 1H), 3.77 (s, 6H), 3.63 (s, 3H), 3.27–3.23 (m, 2H), 2.67 (t, $J$ = 6.0 Hz, 2H), 1.55–1.40 (m, 2H), 0.99 (d, $J$ = 6.1 Hz, 2H). $^{13}$C NMR (100 MHz, DMSO-$d_6$) δ 163.87, 161.53, 158.49, 152.86 (2C), 135.81, 135.79, 119.28, 116.29, 100.05, 60.56, 56.31 (2C), 27.43, 25.95 (2C). HRMS: calcd. for $C_{16}H_{22}BrN_5O_3$: 412.0979 $[M+H]^+$, found: 412.0977.

*4.10.1.24. $N^4$-(3-aminopropyl)-$N^2$-(3,4,5-trimethoxyphenyl)pyrimidine-2,4-diamine (**8b**).* White solid; Yield 68%; m.p. 120–122 °C; $^1$H NMR (400 MHz, DMSO-$d_6$) δ 8.89 (s, 1H), 7.89 (d, $J$ = 7.1 Hz, 1H), 7.83 (s, 1H), 7.12 (s, 2H), 6.30 (d, $J$ = 7.1 Hz, 1H), 3.80 (s, 6H), 3.66 (s, 3H), 2.82 (s, 2H), 1.68–1.54 (m, 4H). $^{13}$C NMR (100 MHz, DMSO-$d_6$) δ 161.10, 159.51, 154.60, 153.26 (2), 134.90, 134.38, 118.98, 116.02, 99.38, 60.60, 56.32 (2), 25.71, 24.90 (2) HRMS: calcd. for $C_{16}H_{23}N_5O_3$: 334.1874 $[M+H]^+$, found: 334.1873.

*4.10.1.25. $N^4$-(3-aminopropyl)-5-iodo-$N^2$-(3,4,5-trimethoxyphenyl)pyrimidine-2,4-diamine (**8c**).* Yellow powder; Yield 65%; m.p. 111–113 °C; $^1$H NMR (400 MHz, DMSO-$d_6$) δ8.30 (s, 1H), 7.78 (s, 2H), 7.01 (s, 2H), 3.78 (s, 6H), 3.66 (s, 3H), 3.31 (d, $J$ = 5.2 Hz, 2H), 2.84–2.69 (m, 2H), 1.77–1.73 (m, 2H). $^1$H NMR (100 MHz, DMSO-$d_6$) δ 159.63, 159.30, 158.96, 158.64, 152.90 (2C), 118.60, 115.65, 102.01, 96.40, 60.60, 56.46 (2C), 38.44, 37.13 (2C). HRMS: calcd. for $C_{16}H_{22}IN_5O_3$: 460.0840 $[M+H]^+$, found: 460.0842.

*4.10.1.26. $N^4$-(2-(diethylamino)ethyl)-$N^2$-(3,4,5-trimethoxyphenyl)pyrimidine-2,4-diamine (**10a**).* White solid; Yield 77%; m.p. 114–106 °C; $^1$H NMR (400 MHz, DMSO-$d_6$) δ 9.09 (s, 1H), 7.81 (d, $J$ = 5.6 Hz, 1H), 7.10 (s, 2H), 6.36 (s, 1H), 5.97 (d, $J$ = 5.7 Hz, 1H), 3.78 (s, 6H), 3.61 (s, 3H), 3.37–3.33 (m, 2H), 2.56–2.51 (m, 2H), 2.49–2.43 (m, 4H), 0.95–0.90 (m, 6H). $^{13}$C NMR (100 MHz, DMSO-$d_6$) δ 162.35, 161.49, 161.03, 156.50, 153.12 (2), 137.17, 132.67, 97.54 (2), 60.55, 56.15 (2), 52.30, 52.01, 47.08 (2), 12.35 (2). HRMS: calcd. for $C_{19}H_{29}N_5O_3$: 376.2343 $[M+H]^+$, found: 376.2341.

*4.10.1.27. $N^4$-(2-(diethylamino)ethyl)-5-iodo-$N^2$-(3,4,5-trimethoxyphenyl)pyrimidine-2,4-diamine (**10b**).* Yellow powder; Yield 72%; m.p. 101–103 °C; $^1$H NMR (400 MHz, DMSO-$d_6$) δ 8.13 (s, 1H), 7.69 (s, 1H), 7.05 (s, 2H), 6.66 (s, 1H), 3.77 (s, 6H), 3.62 (s, 3H), 3.29–3.24 (m, 2H), 2.46–2.48 (m, 2H), 2.45 (s, 4H), 0.88 (s, 6H). $^{13}$C NMR (100 MHz, DMSO-$d_6$) δ 163.92, 158.57, 156.01, 155.59, 152.84 (2C), 135.67, 133.85, 100.19 (2C), 60.50, 56.27 (2C), 52.04, 50.55, 47.07 (2C), 12.28 (2C). HRMS: calcd. for $C_{19}H_{28}IN_5O_3$: 502.1310 $[M+H]^+$, found: 502.1313.

## Declaration of competing interest

The authors declare that they have no known competing

financial interests or personal relationships that could have appeared to influence the work reported in this paper.

## Acknowledgments

We are grateful to Prof. Liang Ouyang and Prof. Jie Liu (Sichuan University) for their critical reviews on this work. This work was financially supported by National Natural Science Foundation of China (Grant No. 81970481), Sichuan Science and Technology Program (Grant No. 2020JDRC0053), Liaoning Province Natural Science Foundation (Grant No. 2019-MS-299) and Liaoning Revitalization Talents Program (Grant No. XLYC1807182).

## Appendix A. Supplementary data

Supplementary data to this article can be found online at https://doi.org/10.1016/j.ejmech.2020.112782.

## References

[1] K.D. Miller, L. Nogueira, A.B. Mariotto, J.H. Rowland, K.R. Yabroff, C.M. Alfano, A. Jemal, J.L. Kramer, R.L. Siegel, Cancer treatment and survivorship statistics, CA A Cancer J. Clin. 5 (2019) 363–385.
[2] W.D. Travis, E. Brambilla, A.P. Burke, A. Marx, A.G. Nicholson, WHO classification of tumours of the lung, pleura, thymus and heart. Lyon: international agency for research on cancer, J. Thorac. Oncol. 10 (2015) 1383–1395.
[3] K. Politi, R.S. Herbst, Lung cancer in the era of precision medicine, Clin. Canc. Res. 21 (2015) 2213–2220.
[4] N. Duma, R. Santana-Davila, J.R. Molina, Non-small cell lung cancer: epidemiology, screening, diagnosis, and treatment, Mayo Clin. Proc. 94 (8) (2019) 1623–1640.
[5] L. Osmani, F. Askin, E. Gabrielson, Q.K. Li, Current WHO guidelines and the critical role of immunohistochemical markers in the subclassification of non-small cell lung carcinoma (NSCLC): moving from targeted therapy to immunotherapy, Semin. Canc. Biol. 52 (2018) 103–109.
[6] B. Levine, D.J. Klionsky, Development by self-digestion: molecular mechanisms and biological functions of autophagy, Dev. Cell 6 (2004) 463–477.
[7] B. Ravikumar, R. Duden, D.C. Rubinsztein, Aggregateprone proteins with polyglutamine and polyalanine expansions are degraded by autophagy, Hum. Mol. Genet. 11 (2002) 1107–1117.
[8] Y. Kabeya, Y. Kamada, M. Baba, H. Takikawa, M. Sasaki, Y. Ohsumi, Atg17 functions in cooperation with Atg1 and Atg13 in yeast autophagy, Mol. Biol. Cell 16 (2005) 2544–2553.
[9] J.M. Park, M. Seo, C.H. Jung, D. Grunwald, M. Stone, N.M. Otto, E. Toso, Y. Ahn, M. Kyba, T.J. Griffin, L. Higgins, D.H. Kim, ULK1 phosphorylates Ser30 of BECN1 in association with ATG14 to stimulate autophagy induction, Autophagy 14 (2018) 584–597.
[10] O. Kapuy, P.K. Vinod, G. Banhegyi, mTOR inhibition increases cell viability via autophagy induction during endoplasmic reticulum stress - an experimental and modeling study, FEBS Open Bio 4 (2014) 704–713.
[11] S. Shoji-Kawata, R. Sumpter, M. Leveno, et al., Identification of a candidate therapeutic autophagy inducing peptide, Nature 494 (2013) 201–206.
[12] T.T. Shi, X.X. Yu, L.J. Yan, H.T. Xiao, Research progress of hydroxychloroquine and autophagy inhibitors on cancer, Canc. Chemother. Pharmacol. 79 (2017) 287–294.
[13] E. Donohue, A. Tovey, A.W. Vogl, S. Arns, E. Sternberg, R.N. Young, M. Roberge, Inhibition of autophagosome formation by the benzoporphyrin derivative verteporfin, J. Biol. Chem. 286 (2011) 7290–7300.
[14] S. Yang, X. Wang, G. Contino, Pancreatic cancers require autophagy for tumor growth, Genes Dev. 25 (2011) 717–729.
[15] C.M. Dower, N. Bhat, M.T. Gebru, L. Chen, C.A. Wills, B.A. Miller, H.G. Wang, Targeted inhibition of ULK1 promotes apoptosis and suppresses tumor growth and metastasis in neuroblastoma, Mol. Canc. Therapeut. 17 (2018) 2365–2376.
[16] E.Y. Chan, A. Longatti, N.C. McKnight, S.A. Tooze, Kinase-inactivated ULK proteins inhibit autophagy via their conserved C-terminal domains using an Atg13-independent mechanism, Mol. Cell Biol. 29 (2009) 157–171.
[17] F. Tang, P.C. Hu, Z.T. Yang, C. Xue, J. Gong, S.X. Sun, L. Shi, S.M. Zhang, Z.Z. Li, C.X. Yang, J.H. Zhang, C.N. Xie, SBI0206965, a novel inhibitor of Ulk1, suppresses non-small cell lung cancer cell growth by modulating both autophagy and apoptosis pathways, Oncol. Rep. 37 (2017) 3449–3458.
[18] L. Zhang, L. Ouyang, Y. Guo, J. Zhang, B. Liu, UNC-51-like kinase 1: from an autophagic initiator to multifunctional drug target, J. Med. Chem. 61 (15) (2018) 6491–6500.
[19] M.B. Lazarus, C.J. Novotny, K.M. Shokat, Structure of the human autophagy initiating kinase ULK1 in complex with potent inhibitors, ACS Chem. Biol. 10 (2015) 257–261.
[20] M.B. Lazarus, K.M. Shokat, Discovery and structure of a new inhibitor scaffold of the autophagy initiating kinase ULK1, Bioorg. Med. Chem. 23 (2015) 5483–5488.
[21] K.J. Petherick, O.J. Conway, C. Mpamhanga, S.A. Osborne, A. Kamal, B. Saxty, I.G. Ganley, Pharmacological inhibition of ULK1 kinase blocks mammalian target of rapamycin (mTOR)-dependent autophagy, J. Biol. Chem. 290 (2015) 11376–11383.
[22] S. Drießen, N. Berleth, O. Friesen, A.S. Löffler, P. Böhler, N. Hieke, B. Stork, Deubiquitinase inhibition by WP1130 leads to ULK1 aggregation and blockade of autophagy, Autophagy 11 (2015) 1458–1470.
[23] D. F Egan, M.G. Chun, M. Vamos, H.X. Zou, J. Rong, C.J. Miller, R.J. Shaw, Small molecule inhibition of the autophagy kinase ULK1 and identification of ULK1 substrates, Mol. Cell. 59 (2015) 285–297.
[24] S. Porey, X. Zhang, S. Bhowmick, V. Kumar Singh, S. Guin, R.S. Paton, D. Maiti, An alkyne linchpin strategy for drug: pharmacophore conjugation: experimental and computational realization of a meta-selective inverse sonogashira coupling, J. Am. Chem. Soc. (2020), https://doi.org/10.1021/jacs.9b10646.
[25] C. Chang, S. Ekins, P. Bahadduri, P.W. Swaan, Pharmacophore-based discovery of ligands for drug transporters, Adv. Drug Deliv. Rev. 58 (2006) 1431–1450.
[26] D.J. Sun, Y.Q. Zhao, S.Y. Zhang, L. Zhang, B. Liu, L. Ouyang, Dual-target kinase drug design: current strategies and future directions in cancer therapy, Eur. J. Med. Chem. (2020), https://doi.org/10.1016/j.ejmech.2019.112025.
[27] J.P. Métivier, B. Cuissart, R. Bureau, A. Lepailleur. The Pharmacophore Network: A Computational Method for Exploring Structure-Activity Relationships from a Large Chemical Data Set.
[28] B.M. Lazarus, C.J. Novotny, K.M. Shokat, Structure of the human autophagy initiating kinase ULK1 in complex with potent inhibitors, ACS Chem. Biol. 10 (2015) 257–261.
[29] D.B. Kitchen, Docking and scoring in virtual screening for drug discovery: methods and applications, Nat. Rev. Drug Discov. 3 (2004) 935–949.
[30] G. Wu, D.H. Robertson, C.L. Brooks, M. Vieth, J. Comput. Chem. 24 (2003) 1549–1562.
[31] L. Ouyang, L. Zhang, S. Zhang, D. Yao, Y. Zhao, G. Wang, L. Fu, P. Lei, B. Liu, Small-molecule activator of UNC-51-Like kinase 1 (ULK1) that induces cytoprotective autophagy for Parkinson's disease treatment, J. Med. Chem. 61 (2018).
[32] L. Ouyang, L. Zhang, L. Fu, B. Liu, A small-molecule activator induces ULK1-modulating autophagy-associated cell death in triple negative breast cancer, Autophagy 13 (2017) 777–778.
[33] D. Sun, L. Zhu, Y. Zhao, Fluoxetine induces autophagic cell death via eEF2K-AMPKmTOR-ULK complex axis in triple negative breast cancer, J. Cell Proliferation. 51 (2017) 12402–12412.